communications physics

ARTICLE

https://doi.org/10.1038/s42005-023-01447-y OPEN

Efficiency limit of transition metal dichalcogenide solar cells

Koosha Nassiri Nazif [1,4], Frederick U. Nitta[1,2,4], Alwin Daus [1,3], Krishna C. Saraswat [1,2] & Eric Pop [1,2]✉

Ultrathin transition metal dichalcogenide (TMD) films show great promise as absorber materials in high-specific-power (i.e., high-power-per-weight) solar cells, due to their high optical absorption, desirable band gaps, and self-passivated surfaces. However, the ultimate performance limits of TMD solar cells remain unknown today. Here, we establish the efficiency limits of multilayer (≥5 nm-thick) MoS_2, $MoSe_2$, WS_2, and WSe_2 solar cells under AM 1.5 G illumination as a function of TMD film thickness and material quality. We use an extended version of the detailed balance method which includes Auger and defect-assisted Shockley-Read-Hall recombination mechanisms in addition to radiative losses, calculated from measured optical absorption spectra. We demonstrate that single-junction solar cells with TMD films as thin as 50 nm could in practice achieve up to 25% power conversion efficiency with the currently available material quality, making them an excellent choice for high-specific-power photovoltaics.

[1] Department of Electrical Engineering, Stanford University, Stanford, CA 94305, USA. [2] Department of Materials Science and Engineering, Stanford University, Stanford, CA 94305, USA. [3] RWTH Aachen University, Aachen 52074, Germany. [4] These authors contributed equally: Koosha Nassiri Nazif, Frederick U. Nitta ✉email: epop@stanford.edu

Transition metal dichalcogenides (TMDs) have recently received growing interest in high-specific-power (i.e., high-power-per-weight) photovoltaics where light weight and high power conversion efficiency (PCE) are strongly desired[1–4]. TMD materials such as MoS_2 and WSe_2 have high optical absorption coefficients, desirable band gaps for use in single-junction and tandem solar cells (~1.0–2.5 eV), and self-passivated surfaces free of dangling bonds, enabling high performance even for ultrathin absorber layers on the order of 100 nm[2,4–6]. Recently, ultrathin TMD solar cells reached high specific power of 4.4 W g^{-1}, on par with established thin-film solar technologies cadmium telluride (CdTe), copper indium gallium selenide (CIGS), amorphous silicon and III-Vs, with the potential to achieve 10× higher specific power upon optimization[4].

Moreover, adopting ultrathin TMD absorber layers minimizes material utilization, therefore helping with sustainable material use and cost reduction. In addition, the chemical and mechanical stability of TMDs[7] promises reliable and long-lasting performance similar to silicon solar panels, while their biocompatibility[8] allows usage in wearable and implantable electronics in contact with the human body. At the same time, rapid developments in the nanoelectronics industry related to TMD growth and device fabrication[9–12] pave the way for low-cost mass production of TMD solar cells, similar to how silicon solar cells benefited in their early days from developments made in the microelectronics industry. It is therefore timely to determine the ultimate performance limits of TMD solar cells, illustrating their potential for next-generation solar cell technology which could be realized after sufficient optimization.

In this work, we establish the fundamental performance limits of single-junction solar cells made of multilayer (bulk, ≥5 nm-thick) MoS_2, $MoSe_2$, WS_2, and WSe_2 absorber films with a realistic analysis based on the Tiedje-Yablonovitch model originally developed for silicon solar cells[13]. This detailed balance model uses material-specific optical absorption data and includes radiative and Auger recombination as well as free carrier absorption, providing material-specific, thickness-dependent performance limits, as opposed to Shockley-Queisser models[2,14], which assume that absorptance steps from zero to unity at the band gap energy. We also improve our predictions beyond the Tiedje-Yablonovitch model by incorporating defect-assisted Shockley-Read-Hall (SRH) recombination, providing thickness-dependent efficiency limits for various material quality levels. As a consequence, we find that up to 25% power conversion efficiency is achievable in ultrathin (~50 nm) single-junction TMD solar cells even with existing material quality, corresponding to ~10× higher power per weight than commercialized solar cell technologies[4]. This already renders TMD photovoltaics an excellent choice for high-specific-power applications such as autonomous drones, electric vehicles, Internet-of-Things devices, and wearable electronics, which are rapidly growing and soon becoming an integral part of our daily life.

Results and discussion

Modeling setup. The extended detailed balance method developed by Tiedje et al. (known as the Tiedje-Yablonovitch model) is used as the basis for this study[13]. The model was originally developed for silicon solar cells to provide an accurate estimate of their efficiency limits by incorporating the optical absorption characteristics of silicon, radiative and Auger recombination, and free carrier absorption. In this study, we go beyond the Tiedje-Yablonovitch model and investigate the effect of material quality on solar cell performance by including defect-assisted SRH recombination, as detailed in Supplementary Note 1. This comprehensive model provides efficiency limits of single-junction, multilayer (≥5 nm-thick) TMD (MoS_2, $MoSe_2$, WS_2, and WSe_2) solar cells as a function of TMD film thickness and quality.

To mimic optimal light trapping, a rectangular slab of multilayer MoS_2, $MoSe_2$, WS_2, and WSe_2 with a perfect anti-reflection coating on the front surface (zero reflection) and a perfect back-reflector (unity reflection) is considered (Fig. 1). The illumination (AM 1.5 G spectrum with one-sun intensity) includes both direct and diffuse sunlight over a full 2π-steradian acceptance angle, appropriate for a non-tracking flat solar panel. In the Tiedje-Yablonovitch model[13], the surfaces are assumed to be textured non-specular (Lambertian), e.g., created by etching, leading to randomized light and angle-independent absorption. For absorber layers that are many wavelengths thick ($L >> \lambda$, where λ is the wavelength), as in the case of thick

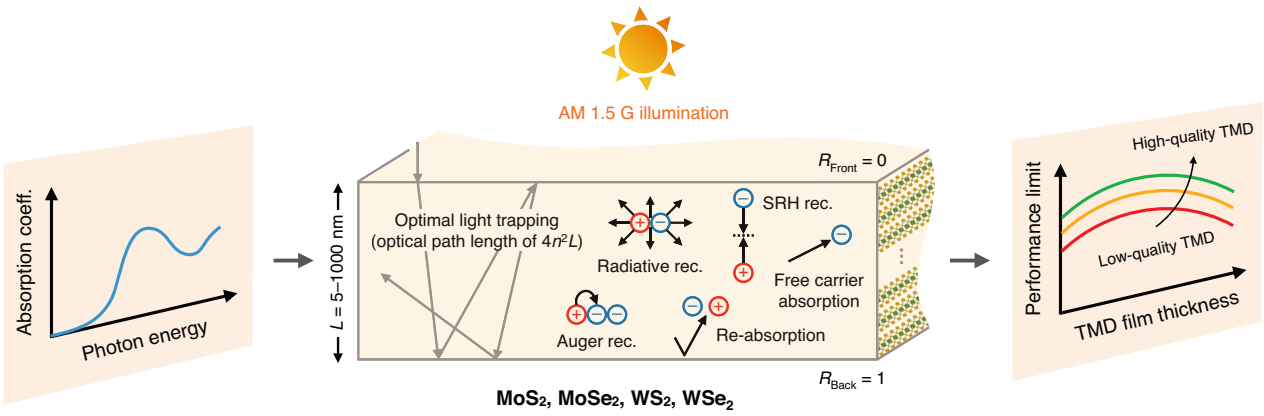

Fig. 1 Modeling setup. Schematics of input optical absorption coefficient spectrum, solar cell geometry, multilayer transition metal dichalcogenides (TMDs) modeled, incident sunlight, absorption assumptions, recombination mechanisms, and output thickness- and material quality-dependent performance limits. *R*, reflection; *L*, TMD film thickness; *n*, refractive index; SRH rec., Shockley-Read-Hall recombination. Anti-reflection coating on the front surface yields zero reflection ($R_{Front} = 0$). The back-reflector, which exhibits unity reflection ($R_{Back} = 0$), could be either flat (mirror) or patterned with periodic grating structures. The assumed optical path length of $4n^2L$ (absorption enhancement factor of $4n^2$) is a conservative upper limit for light trapping in nanoscale films with thicknesses comparable to or smaller than the wavelength scale, which can be achieved in practice with proper design[16]. Photogenerated excitons, which exhibit small (~0.05 eV) binding energies in multilayer TMDs[29,30], are instantly dissociated into free electrons and holes under the electric field present in well-designed multilayer TMD solar cells[31,32].

(~100 μm) silicon solar cells in the original Tiedje-Yablonovitch study[13], this gives a mean path length of $4n^2L$ (absorption enhancement factor of $4n^2$) for light rays in the semiconductor[13,15], calculated using the conventional ray optics model, where L is the film thickness and n is the semiconductor refractive index.

For nanoscale films with thicknesses comparable to or smaller than the wavelength scale (e.g., the 5 nm–1 μm TMD films studied here), some of the basic assumptions of the conventional theory are no longer applicable[13,16]. To address this, Yu et al.[16] developed a statistical coupled-mode theory that describes light trapping in general from a rigorous electromagnetic perspective, showing that the absorption enhancement factor in nanoscale films can go far beyond the $4n^2$ bulk limit with proper design. As an example, the authors numerically demonstrated a light-trapping scheme for a 5 nm film leading to an absorption enhancement factor of $12 \times 4n^2$ over a virtually unlimited spectral bandwidth and with near-isotropic angular response. We can therefore conclude that $4n^2$ is a conservative upper limit for absorption enhancement in the nanoscale films considered here. Nevertheless, given the dependence of absorption enhancement in nanoscale films on the chosen light trapping scheme (e.g., mirrors, periodic structures, scattering or cladding layers, etc.)[16], in this study we use $4n^2$ enhancement factor as a baseline for optimal light trapping, which can be achieved in practice with proper design. Because n is relatively constant across all wavelengths of interest[17], we use the n value at the band gap energy. The operating temperature is assumed to be 300 K.

Radiative, Auger, and SRH recombination mechanisms are all considered (Fig. 1), as described in Supplementary Note 1. Measured optical absorption coefficient spectra of bulk TMDs[17] (Supplementary Fig. 1) are used to accurately calculate both absorptance and the radiative losses, and to extract the optical band gap of TMD films using the Tauc method[18] (Supplementary Fig. 2). SRH lifetime (τ_{SRH}) is varied from 1 ns to infinity (the case in the Tiedje-Yablonovitch model) to determine efficiency limits at various material quality levels. Auger coefficients are extrapolated from Auger coefficient–band gap charts in the literature[19]. Intrinsic or lightly doped TMDs are considered such that hole and electron densities are equal under illumination. At low doping densities, free carrier absorption is negligible in ultrathin absorbers[20]. We therefore exclude free carrier absorption from our analysis. A summary of modeling parameters is listed in Table 1. The model outputs the performance limits of the solar cell, particularly the power conversion efficiency, as a function of TMD film thickness and material quality.

Another important loss mechanism in solar cells is surface recombination, which could be eliminated by suitable passivation treatments[13]. TMDs have the unique advantage of dangling-bond-free, self-passivated surfaces thanks to their van der Waals, layered structure. In the absence of defects at the TMD interfaces with other materials (e.g., the contacts), these surfaces can guarantee near-zero surface recombination. In the presence of defects, conventional passivation techniques such as the use of oxides, are shown[5,21] to effectively passivate surface defects in TMDs and achieve near-zero surface recombination. We therefore assume zero surface recombination in optimally-designed TMD solar cells reaching the efficiency limits, and exclude surface recombination from our analysis. Nevertheless, the results are valid even in the presence of surface recombination. This is because the SRH lifetime in our model could be considered an effective recombination lifetime representing both bulk SRH and surface recombination. This particularly reflects the SRH lifetime measurements in thin absorber films, where the results are influenced by surface recombination and hence represent the effective lifetime rather than the SRH lifetime[22].

We note that excitons play a key role in the optoelectronic characteristics of TMDs, particularly in the monolayer limit. Due to quantum confinement effects and reduced Coulomb screening, monolayer TMDs exhibit[23] large exciton binding energies >0.5 eV. These binding energies are one order of magnitude larger than the room-temperature thermal energy, limiting thermal or spontaneous dissociation even at elevated temperatures and exciton densities. It is therefore essential to include the dynamics of exciton dissociation in power conversion efficiency models for monolayer TMDs[24–28].

On the other hand, multilayer or bulk TMDs (≥5 nm-thick) which are the focus of our study, show[29,30] significantly smaller exciton binding energies around 0.05 eV, comparable to the room-temperature thermal energy, leading to rapid dissociation upon generation[31,32]. Femtosecond pump–probe spectroscopy measurements on few-layer WS_2 show[31] efficient exciton dissociation with a characteristic time of 1.3 ps. The presence of a weak-to-moderate electric field, as guaranteed in a well-designed solar cell reaching the efficiency limits, results in even faster exciton dissociation. Pedersen et al. showed[32] that in-plane or out-of-plane electric fields as low as 10 mV/nm yield dissociation rates as high as 10^{13} s^{-1} in bulk WSe_2, WS_2, $MoSe_2$, and MoS_2. These exciton dissociation rates are 3–4 orders of magnitude faster than exciton recombination rates in multilayer TMDs[33–36]. We therefore assume here that photogenerated excitons are instantly dissociated into free electrons and holes before recombination, similar to 3D semiconductor solar cells such as Si and GaAs.

Spectral absorptance. To highlight the unusually high light absorption in thin TMD films, we calculate the spectral absorptance of multilayer MoS_2, $MoSe_2$, WS_2, and WSe_2 films with an absorption enhancement factor of $4n^2$ (as achieved by the

Table 1 Modeling parameters for bulk MoS_2, $MoSe_2$, WS_2, and WSe_2[17,19,29,30,50].

Material	MoS_2	$MoSe_2$	WS_2	WSe_2
Band gap, E_G (eV)	1.27	1.16	1.36	1.29
Refractive index at E_G, n	4.48	3.67	4.68	4.63
Exciton binding energy, E_b (eV)	0.050	0.067	0.050	0.050
Effective electron mass, m_e^*	$0.71m_e$	$0.64m_e$	$0.63m_e$	$1.00m_e$
Effective hole mass, m_h^*	$0.84m_e$	$0.97m_e$	$0.84m_e$	$0.59m_e$
Effective conduction band density of states, N_C (cm^{-3})	1.50×10^{19}	1.29×10^{19}	1.26×10^{19}	2.51×10^{19}
Effective valence band density of states, N_V (cm^{-3})	1.93×10^{19}	2.40×10^{19}	1.93×10^{19}	1.14×10^{19}
Intrinsic carrier concentration, n_i (cm^{-3})	3.70×10^{8}	3.20×10^{9}	5.93×10^{7}	2.49×10^{8}
Auger recombination coefficient (cm^6 s^{-1})	$10^{-29.7}$	$10^{-29.3}$	$10^{-30.0}$	$10^{-29.7}$

Effective masses and densities of states are appropriately averaged over the in-plane and cross-plane TMD components.

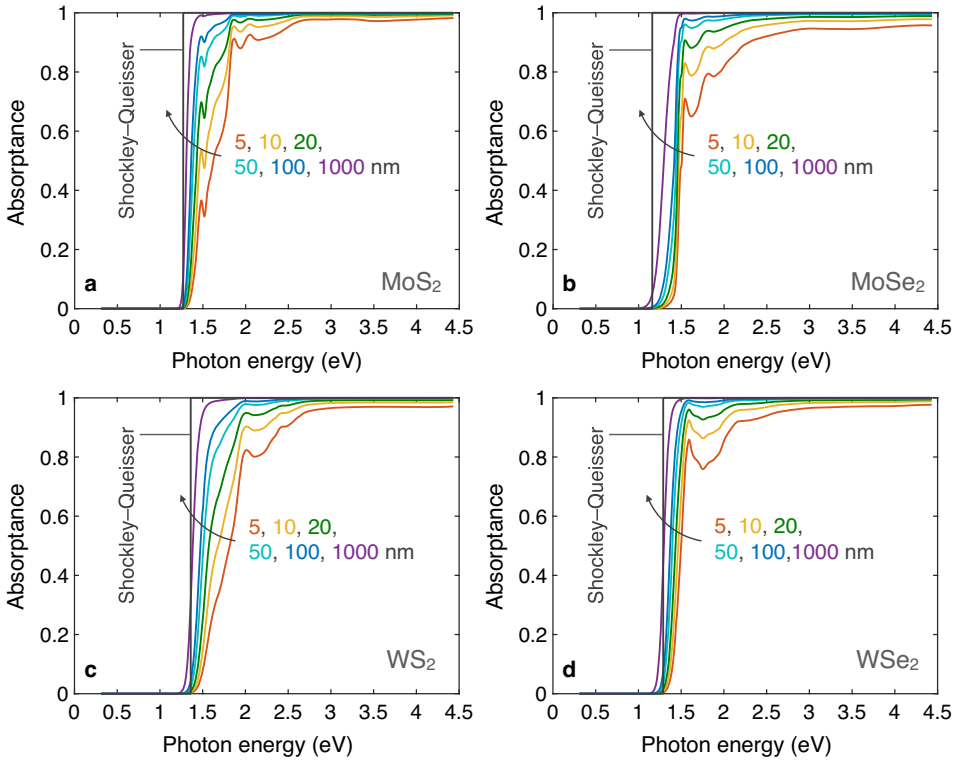

Fig. 2 Light absorptance in thin TMD films. Spectral absorptance of **a** MoS_2, **b** $MoSe_2$, **c** WS_2, and **d** WSe_2 films with an absorption enhancement factor of $4n^2$ (as achieved by the setup shown in Fig. 1) at various thicknesses between 5 and 1000 nm, along with the step-function Shockley-Queisser model. The Tauc band gap[18] of the materials is used for the Shockley-Queisser model (see Supplementary Fig. 2).

setup shown in Fig. 1) at 5, 10, 20, 50, 100, and 1000 nm film thickness (Fig. 2) using their measured optical absorption coefficient spectra[17] (Supplementary Fig. 1). Due to their large absorption coefficients and refractive indices, all these TMDs exhibit significant light absorptance even in ultrathin films of 5 nm thickness (Fig. 2), four orders of magnitude thinner than conventional silicon solar cell absorber layers (~200 µm). As the thickness approaches 1000 nm, the absorptance approaches the simplified step-function assumption in the Shockley-Queisser model[14], with exponential Urbach tails[37] arising from exciton-phonon and exciton-defect interactions in TMDs[38]. The absorptance peaks are mainly attributed to the A and B excitons in these materials[39] (Supplementary Fig. 1).

The relative absorptance of the four TMDs can be explained by their respective absorption coefficient spectra (Supplementary Fig. 1), particularly in the 1–2.5 eV range, and by their refractive indices (Table 1). Selenides ($MoSe_2$ and WSe_2) have larger absorption coefficients than the sulfides (MoS_2 and WS_2), leading to steeper and higher absorptance in the 1–2.5 eV regime, beyond which near-unity absorptance is reached in all four TMDs, even in ultrathin films of only 5 nm thickness. WSe_2 has a larger refractive index, and thus longer optical path length ($4n^2L$) compared to $MoSe_2$, leading to the highest absorptance among the four TMDs. On the other hand, WS_2 has the smallest absorption coefficient in the 1–2.5 eV range, with a refractive index comparable to MoS_2, therefore making it the least light-absorptive of the four TMDs.

Short-circuit current density. Figure 3 shows the calculated short-circuit current density (J_{SC}) of TMD solar cells as a function of the TMD (absorber) film thickness. As expected from their exceptional light absorption characteristics, all TMDs can achieve high J_{SC} even at small thicknesses.

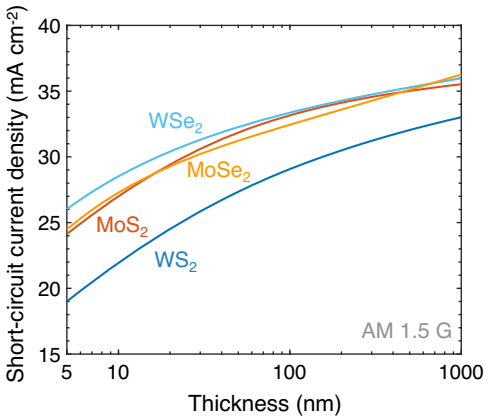

Fig. 3 Short-circuit current densities of thin-film TMD solar cells. Short-circuit current densities of MoS_2, $MoSe_2$, WS_2, and WSe_2 solar cells as a function of the TMD (absorber) film thickness, at 300 K and AM 1.5 G illumination.

Absorptance and therefore J_{SC} increase with increasing TMD film thickness. Radiative, Auger, and SRH recombination do not affect the J_{SC} limits within the thickness and SRH lifetime ranges modeled here, particularly due to the low carrier density at zero bias in the intrinsic or lightly-doped TMDs assumed (see Supplementary Note 1 for more details). In the simple detailed balance Shockley-Queisser model, semiconductors with smaller band gap exhibit higher J_{SC}, because they absorb a larger portion of the AM 1.5 G spectrum, with photon energies above their band gap. However, as evident in Fig. 3, this is not necessarily true with the extended Tiedje-Yablonovitch method, where absorptance is determined by optical absorption

coefficient and refractive index. We observe that J_{SC} follows the same trend as absorptance, with WSe_2 and WS_2 showing the highest and lowest J_{SC}, respectively, and $MoSe_2$ and MoS_2 in between.

We also note a change in slope of the J_{SC} trends in Fig. 3, where J_{SC} increases more strongly at smaller thicknesses, but then rises at a lower rate in thicker films. The initial steeper J_{SC} increase with thickness can be explained by the noticeable absorptance enhancement (Fig. 2) in the ~1.5–2.5 eV regime as the TMD film thickness approaches ~20 nm ($MoSe_2$ and WSe_2) to ~50 nm (MoS_2 and WS_2). Beyond these thicknesses, the absorptance improvement in the ~1.5–2.5 eV region is less prominent. Note that the absorption threshold shifts by approximately 0.2 eV to lower energies as the film thickness increases from 5 nm to 1000 nm (see Fig. 2). This shift is the main driver for the continued, yet gentler J_{SC} increase beyond ~20 nm (~50 nm) in $MoSe_2$ and WSe_2 (MoS_2 and WS_2). The absorption threshold shift is more pronounced in $MoSe_2$ (Fig. 2), enabling it to achieve larger J_{SC} than MoS_2 and WSe_2 at large thicknesses beyond ~600 nm.

Luminescent emission rates. Examining the radiative losses, Fig. 4 shows the spectral dependence of the luminescent emission rates for 100 nm-thick TMD films in thermal equilibrium at 300 K, as described in Supplementary Note 2. One can observe that reabsorption is almost equally probable as external emission in MoS_2. Moreover, the radiative loss is primarily from the low-energy (long-wavelength) photons, which have higher absorption depth and therefore lower probability of being reabsorbed into the TMD film. Similar behavior is observed in $MoSe_2$, WS_2, and WSe_2, with external emission occurring at lower photon energies (longer wavelengths) and reabsorption taking place at higher photon energies (shorter wavelengths). The magnitude of emission rates varies among the four TMDs due to the difference in their absorption coefficients and refractive indices. As detailed in Supplementary Note 2, at equilibrium, the internal emission rate is proportional to the absorption coefficient and the square of the refractive index. For example, $MoSe_2$ has a noticeably higher absorption coefficient than other TMDs in the 1–1.3 eV range due to its smaller band gap (1.16 eV), leading to the highest internal emission rates. The opposite holds true for WS_2, which has the largest band gap (1.36 eV) and smallest absorption coefficient in the entire 1–1.6 eV range (Supplementary Fig. 1). The reabsorption rate is equal to the product of the internal emission rate and the absorptance (Fig. 2). Finally, the external emission rate, in the absence of free carrier absorption, is the difference between the rates of internal emission and reabsorption.

Open-circuit voltage. The calculated open-circuit voltage (V_{OC}) of TMD solar cells as a function of TMD film thickness and material quality (SRH lifetime, τ_{SRH}) is shown in Fig. 5, along with the estimate from the Shockley-Queisser model. Infinite SRH lifetime corresponds to the Tiedje-Yablonovitch model where defect-assisted SRH recombination is excluded. The Shockley-Queisser results were generated from the Tiedje-Yablonovitch model by setting a step-function absorptance (from zero to unity at the band gap) and excluding Auger recombination. The results (shown in Supplementary Table 1) perfectly match with previous Shockley-Queisser reports[40], confirming the accuracy of our Tiedje-Yablonovitch model and code.

We observe that radiative and Auger losses have comparable contributions (Supplementary Fig. 3), similar to the case of Si in the original Tiedje-Yablonovitch study[13], with radiative loss showing a relatively higher contribution due to the higher absorption coefficient in TMDs. Radiative and Auger mechanisms both have recombination lifetimes >10 µs in the multilayer TMDs studied here (Supplementary Fig. 3), which are 2–4 orders of magnitude larger than in direct band gap monolayer TMDs[41,42]. These results agree well with previous reports of photoluminescence quantum yield (PLQY) in monolayer and multilayer TMDs[2,41]. PLQY, the ratio of radiative recombination over total recombination[43], approaches near unity in monolayer TMDs thanks to their direct band gaps, but is only 10^{-4} to 10^{-2} in multilayer TMDs, which have dominant non-radiative recombination due to their indirect band gaps[2,41]. The measured SRH lifetimes[3,44] of ~20–600 ns and PLQY values[2] of 10^{-4} to 10^{-2} verify the 10–100 µs radiative lifetime values calculated here. In Fig. 5, we demonstrate the noticeable effect of material quality on V_{OC} for τ_{SRH} smaller than 10 µs where SRH recombination starts to dominate the V_{OC} loss. Among these four TMDs, we note that WS_2 has the largest V_{OC} for any given τ_{SRH}, due to its largest band gap among the TMDs investigated here. Incidentally, an SRH lifetime up to ~611 ns has also been reported[3] for multilayer WS_2, although lifetimes for this and other TMDs are all expected to increase as the material quality improves. Applied to the materials studied here, such an SRH lifetime would lead to a V_{OC} limit between 0.8 to 1.0 V in 100 nm-thick TMD solar cells.

The largest V_{OC} reported to date in single-junction multilayer TMD solar cells under AM 1.5 G illumination is 0.7 V, demonstrated in p–n junction WS_2 and locally-gated $MoSe_2$ solar cells[5,45], the latter approaching the V_{OC} limit predicted by our model. Given the ~7-nm $MoSe_2$ film thickness in the study[45] and the measured SRH lifetimes of ~20–600 ns reported in the literature for bulk TMDs[3,44], our model predicts a V_{OC} limit of ~0.7–0.9 V (Fig. 5b). The small discrepancy between the predicted V_{OC} limit and the experimentally demonstrated V_{OC} could be due to various sources including the suboptimal choice of contact metals (Ti/Au for both n- and p-contacts), surface recombination, and incomplete exciton dissociation which is not included in our model. Svatek et al. have demonstrated[46] V_{OC} of 1.02 V in a 120 nm-thick p–n junction MoS_2 solar cell under broadband illumination with 4 W cm^{-2} power intensity (equivalent to 40-sun intensity). Given the logarithmic dependence of V_{OC} on light intensity, this corresponds to a V_{OC} of ~0.9 V under 1-sun illumination, which is on par with the V_{OC} limit predicted by our model for a τ_{SRH} of 611 ns (Fig. 5a), demonstrating the feasibility of achieving the performance limits predicted in this study by an optimized design.

We note that for thin TMD films, our model estimates a larger V_{OC} limit than the simpler Shockley-Queisser model for τ_{SRH} larger than 1 µs. This is due to our inclusion of measured optical absorption spectra. As can be seen in Fig. 2, the absorption threshold depends on the thickness and occurs at higher photon energies in thinner TMD films, yielding an effectively larger band gap than the simple Shockley-Queisser model, a discrepancy that becomes greater for thinner films. This highlights the inadequacy of the step-function absorption assumption in the Shockley-Queisser model, where only one threshold (band gap) energy is used for all film thicknesses. This negative shift in absorption threshold with increasing thickness also explains why V_{OC} decreases as the thickness increases.

Fill factor. We also investigate the effect of TMD film thickness and material quality on the fill factor of the four types of TMD solar cells in Fig. 6. It is well-known that the larger the V_{OC}, the higher the fill factor of the solar cell[47]. Therefore, WS_2, having the largest band gap and V_{OC}, shows the highest fill factor, and

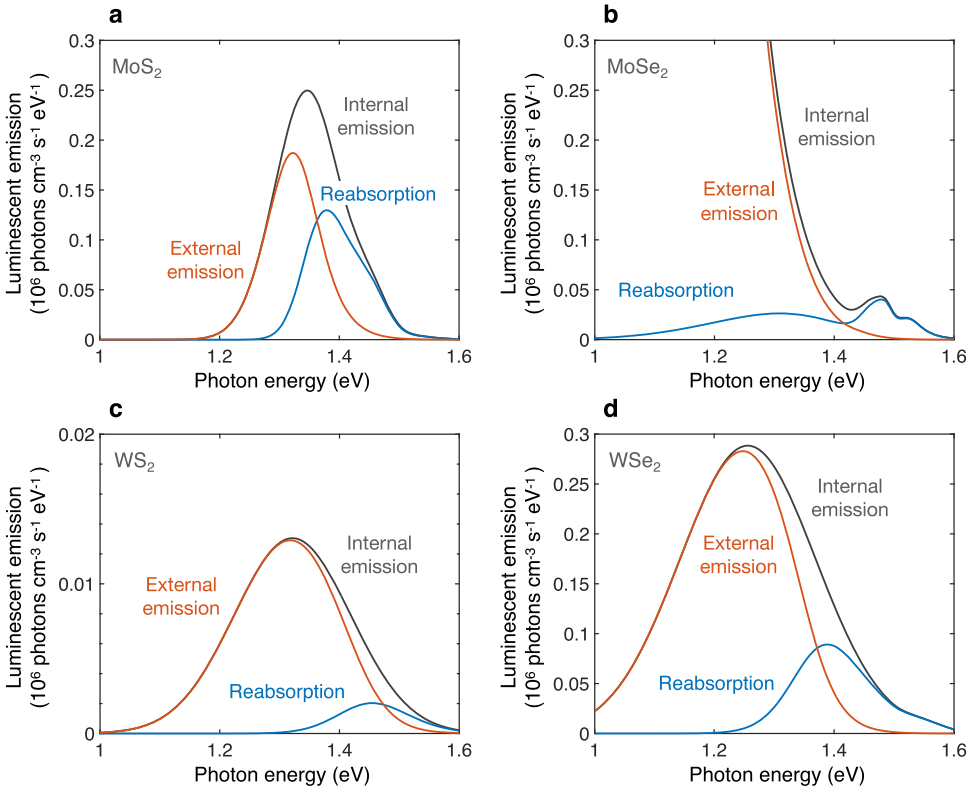

Fig. 4 Luminescent emission rates. Spectral dependence of the luminescent emission rates for a 100 nm-thick film of **a** MoS_2, **b** $MoSe_2$, **c** WS_2, and **d** WSe_2 in thermal equilibrium at 300 K. Note the vertical axis for WS_2 (**c**) is smaller than the vertical axes of the other three panels.

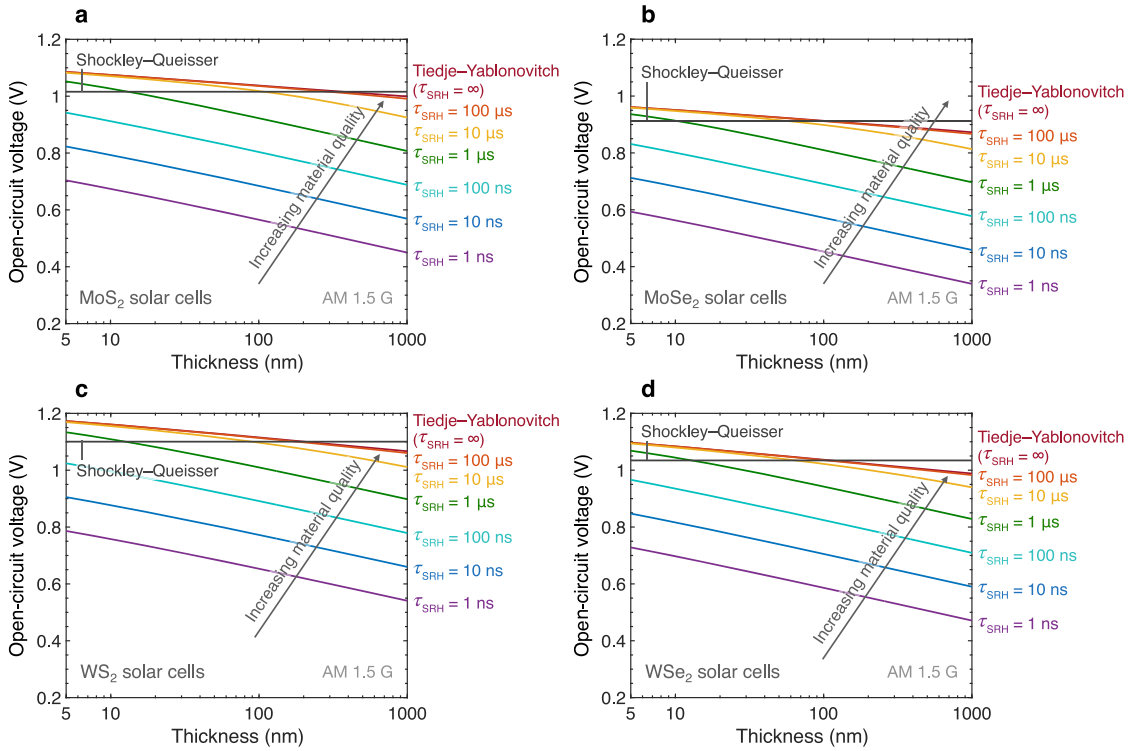

Fig. 5 Open-circuit voltage of thin-film TMD solar cells. Open-circuit voltage of **a** MoS_2, **b** $MoSe_2$, **c** WS_2, and **d** WSe_2 solar cells as a function of TMD film thickness and material quality (τ_{SRH}), at 300 K and AM 1.5 G solar illumination. τ_{SRH}, Shockley-Read-Hall (SRH) lifetime.

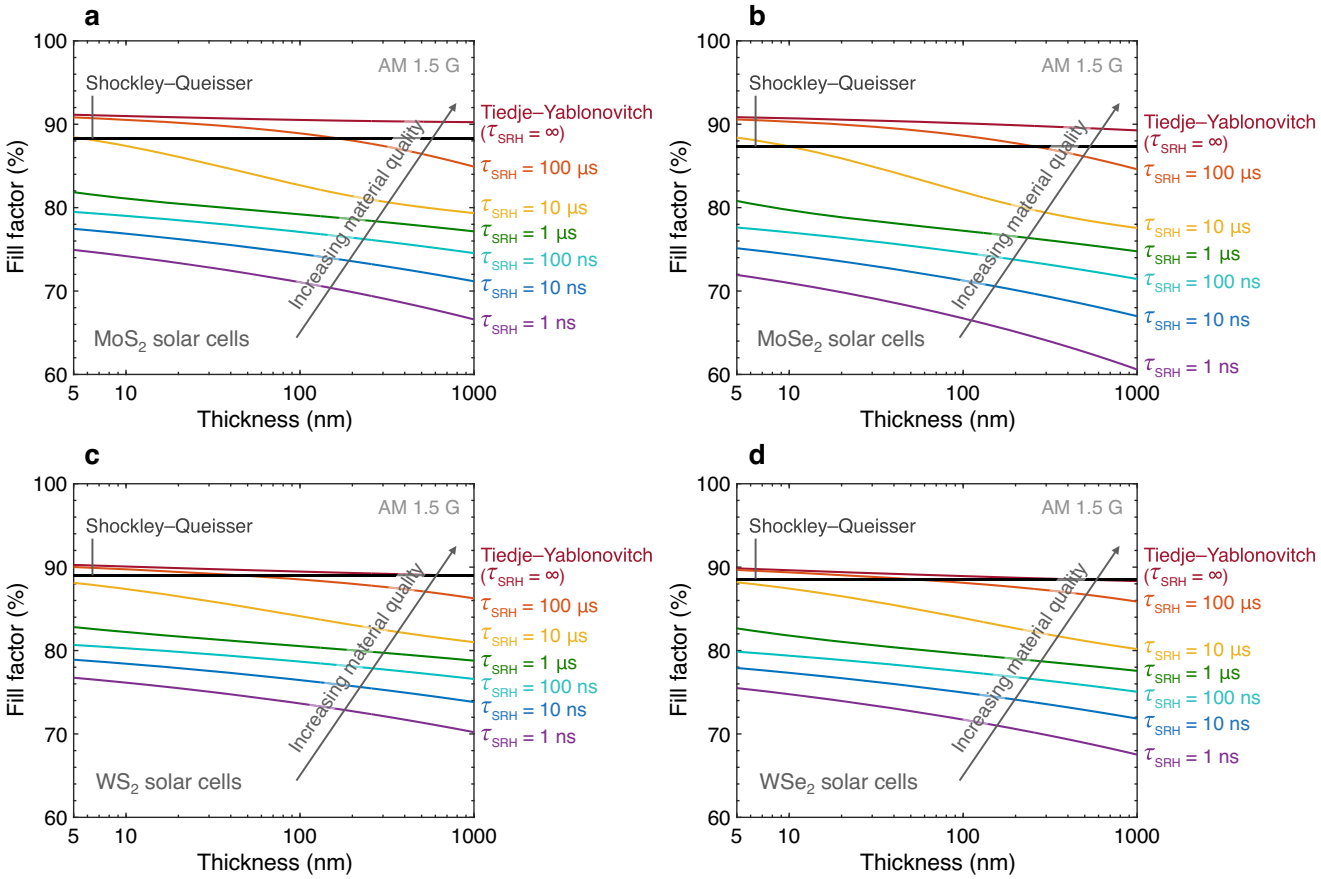

Fig. 6 Fill factor of thin-film TMD solar cells. Fill factor of **a** MoS_2, **b** $MoSe_2$, **c** WS_2, and **d** WSe_2 solar cells as a function of TMD film thickness and material quality (τ_{SRH}), at 300 K and AM 1.5 G solar illumination. τ_{SRH}, Shockley-Read-Hall (SRH) lifetime.

$MoSe_2$, which has the smallest band gap and V_{OC}, exhibits the lowest fill factor among the four TMDs. The fill factor dependence on V_{OC} also explains why fill factor decreases with increasing thickness (due to the negative shift in absorption threshold) and decreasing material quality—following the same trend as V_{OC} (Fig. 5). Studies also show that the closer the solar cell (diode) ideality factor to unity, the higher the fill factor[47], which explains the higher fill factor in the absence of SRH recombination ($\tau_{SRH} \to \infty$) compared to the case where $\tau_{SRH} =$ 100 µs even though the two have essentially the same V_{OC}. Dominant SRH recombination (i.e., $\tau_{SRH} < 10$ µs) leads to an ideality factor of 2 at high-level injection[48,49], which is the case here since the semiconductor is assumed intrinsic or lightly-doped, whereas dominant Auger recombination gives an ideality factor of 2/3[48,49], leading to higher fill factor.

Power conversion efficiency. Most importantly, Fig. 7 shows the power conversion efficiency of MoS_2, $MoSe_2$, WS_2, and WSe_2 solar cells as a function of TMD film thickness and material quality (i.e., SRH lifetime, τ_{SRH}). The Shockley-Queisser efficiency limits are included for comparison. Given that efficiency is equal to the product of J_{SC}, V_{OC}, and fill factor, the efficiency trends observed in Fig. 7 can be easily explained by J_{SC}, V_{OC}, and fill factor trends in Figs. 3, 5, and 6, respectively. As the TMD film thickness increases, absorptance and therefore J_{SC} improve (Fig. 3), whereas both V_{OC} (Fig. 5) and fill factor (Fig. 6) degrade due to the negative shift in absorption threshold. This competition causes the inverted U-shaped curves in Fig. 7, where efficiency initially increases with thickness and then decreases after a certain point. With the Tiedje-Yablonovitch model ($\tau_{SRH} \to \infty$), the maximum efficiency occurs for thicknesses over 1000 nm, therefore we only observe an increasing trend within the range of thicknesses considered here. At 100 nm absorber layer thickness, TMD solar cells achieve up to ~31% Tiedje-Yablonovitch efficiency (Supplementary Table 2), which is ~5% higher than the Tiedje-Yablonovitch efficiency limit of silicon solar cells (29.8%) with 1000 times thicker absorber layers (100 µm). This highlights the considerable potential of TMD solar cells for ultrathin photovoltaics with high power per weight.

Going beyond the Tiedje-Yablonovitch model, we introduce non-negligible SRH recombination (i.e., reduced τ_{SRH}, corresponding to reduced material quality), observing how the efficiency drops in Fig. 7, as a consequence of V_{OC} and fill factor degradation (Figs. 5 and 6). Moreover, we note that for smaller τ_{SRH} the maximum efficiency in Fig. 7 occurs at smaller thicknesses since stronger SRH recombination leads to steeper degradation in V_{OC} and fill factor with increasing film thickness. In other words, although the peak efficiency is reduced, one benefit of "more defective" TMD materials is that their efficiency is maximized in a thinner material, which could potentially have higher specific power and lower cost.

Another way to visualize the effect of material quality (τ_{SRH}) on the solar cell performance is to look at current density–voltage (J–V) characteristics for a fixed thickness, for example, 100 nm (Supplementary Fig. 4). As noted previously, within the thickness and τ_{SRH} ranges considered here, SRH recombination does not influence J_{SC} due to the low carrier density at zero bias in the intrinsic or lightly-doped TMDs assumed, but it impacts both V_{OC} and fill factor, therefore power conversion efficiency. We

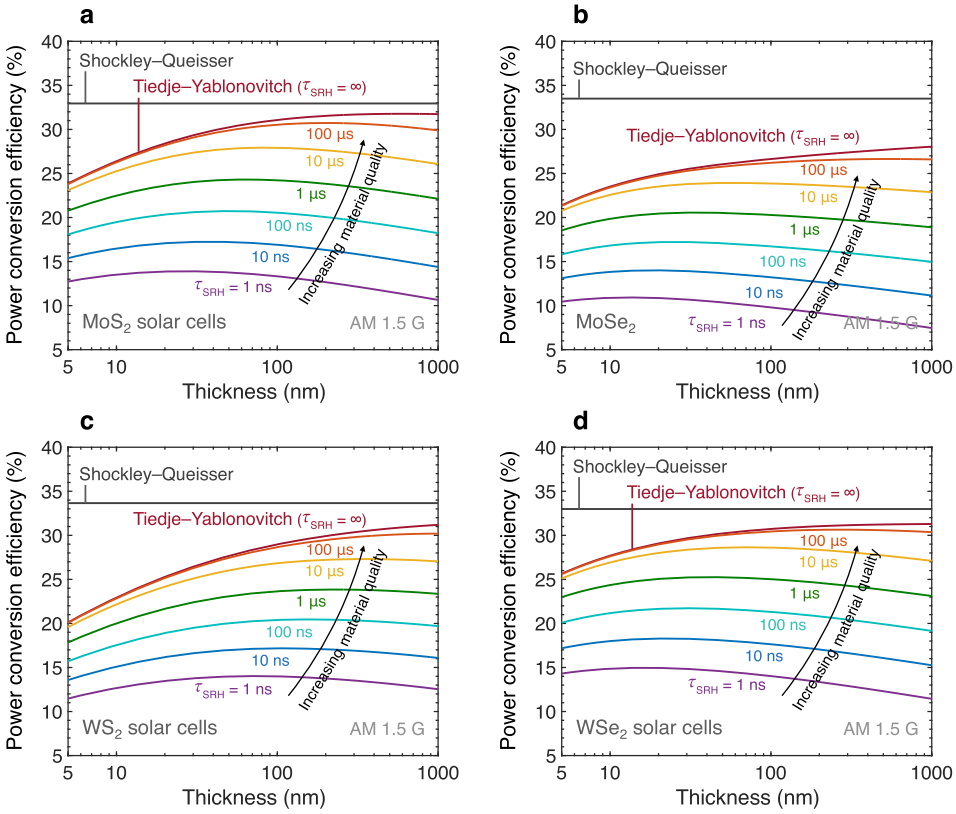

Fig. 7 Power conversion efficiency of thin-film TMD solar cells. Power conversion efficiency of **a** MoS_2, **b** $MoSe_2$, **c** WS_2, and **d** WSe_2 solar cells as a function of TMD film thickness and material quality (τ_{SRH}), at 300 K and AM 1.5 G solar illumination. τ_{SRH}, Shockley-Read-Hall (SRH) lifetime.

also examine the effect of Auger recombination on power conversion efficiency, varying the Auger coefficients of TMDs in the absence of SRH recombination by four orders of magnitude (Supplementary Fig. 5), two orders of magnitude below and above the primary Auger coefficients used in this study, which were extrapolated from Auger coefficient–band gap charts in the literature[19]. We observe that such a large variation in Auger coefficients leads to a mere 1–2% change in power conversion efficiency, demonstrating the robustness of the efficiency limits modeled in this study despite the uncertainty over the exact Auger coefficient values.

The relative efficiencies of the four TMDs can be explained by their relative J_{SC}, V_{OC}, and fill factors. In the 100 ns–1 µs SRH lifetime regime, WSe_2 solar cells demonstrate the highest efficiency, followed by MoS_2, WS_2, and $MoSe_2$ solar cells. Our WS_2 results agree with previous simulation studies on multilayer WS_2 solar cells having a particular design structure (i.e., with back-reflector, transparent conductive oxide contacts, and a front glass shield), which achieve ~15% efficiency with a ~500 nm-thick WS_2 absorber layer having 10–100 ns charge carrier lifetime[26]. To date, SRH lifetimes up to 611 ns are reported in the literature for multilayer TMDs[3], corresponding to ~20–25% power conversion efficiency for the TMD solar cells examined here with ultrathin films of 20–100 nm thickness (Fig. 7). Such power conversion efficiency can be practically achieved by optimizing the optical and electrical design of the ultrathin TMD solar cells, yielding 57–71 W g^{-1} specific power in a packaged cell (Supplementary Fig. 6), ~10× higher than established solar cell technologies such as III–Vs, CdTe and CIGS[4]. Packaged TMD solar cells could be used in low-power, size-constrained applications like Internet of Things (IoT) and wearable electronics. High-power applications, however, such as drones, low-earth-orbit satellites, and electric vehicles require large solar modules consisting of numerous solar cells, which exhibit noticeably higher areal densities due to the inclusion of thick module encapsulation layers as well as interconnects[1]. 20–25% efficient TMD solar cells can achieve 2.6–3.3 W g^{-1} specific power in a fully packaged module (Supplementary Fig. 6), which is approximately 5× higher than high-specific-power solar modules currently on the market[1]. Such lightweight TMD solar cells and modules could create unprecedented opportunities across various industries from aerospace to wearable electronics.

Loss mechanisms at play. Finally, Fig. 8 summarizes the relative magnitudes of various loss mechanisms in optimized 100 nm-thick TMD solar cells at the maximum power point (MPP), as detailed in Supplementary Note 1. τ_{SRH} of 100 µs is considered, where SRH recombination has comparable carrier lifetime and therefore magnitude with Auger and radiative losses (Supplementary Table 3). At shorter τ_{SRH}, SRH recombination dominates and accounts for nearly all the recombination loss, as can be seen in Figs. 5–7. At a fixed τ_{SRH}, the relative magnitudes of SRH recombination in various TMDs depend on their carrier densities (Supplementary Note 1). At their maximum power point, 100 nm-thick MoS_2 and WS_2 have the highest and lowest carrier densities (Supplementary Table 3), and therefore the largest and smallest current loss due to the SRH recombination.

Internal emission scales exponentially with the output voltage (Supplementary Note 1). As a result, $MoSe_2$ which has the smallest band gap and therefore V_{MPP} (Supplementary Table 3), shows the smallest internal emission despite its relatively higher absorption coefficient. For each TMD, the relative magnitudes of reabsorption and external emission are the same as in Fig. 4. Auger loss is proportional to Auger coefficient and the cube of

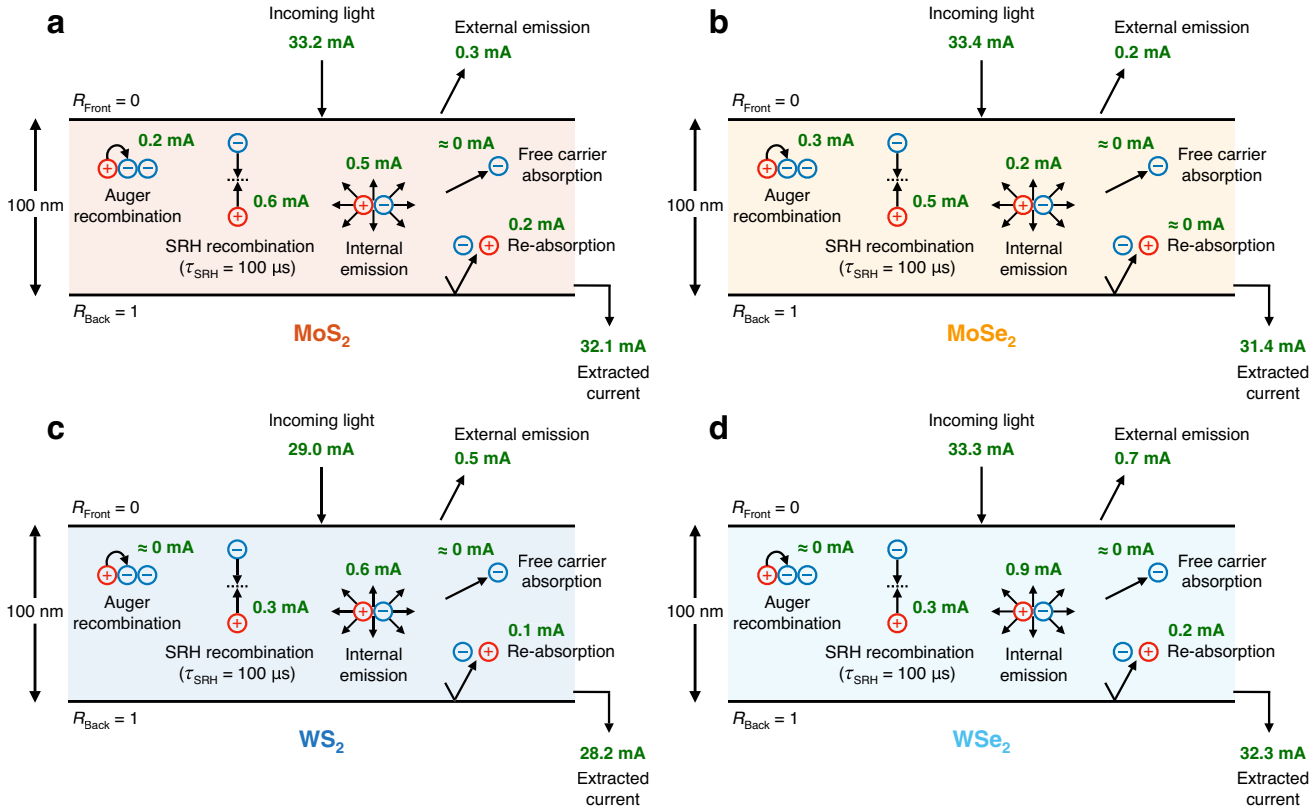

Fig. 8 Loss mechanisms at play. Summary of relative magnitudes of various loss mechanisms in 100 nm-thick **a** MoS_2, **b** $MoSe_2$, **c** WS_2, and **d** WSe_2 solar cells at the maximum power point, 300 K temperature, and AM 1.5 G solar illumination. Shockley-Read-Hall (SRH) lifetime, $\tau_{SRH} = 100$ µs is considered. The solar cells are assumed to have optimized electrical and optical design. Free carrier absorption is negligible given the low doping density and small thickness of the TMDs assumed here[20]. *R*, reflection.

carrier density at the maximum power point (Supplementary Note 1), therefore smallest for WS_2 and WSe_2 (see Table 1 and Supplementary Table 3). As discussed previously, free carrier absorption is negligible due to the low doping density and small thickness of the TMDs assumed here[20]. The relative magnitudes of SRH, Auger and radiative recombination in each TMD can be explained by their relative carrier lifetimes, given the inverse proportionality between the recombination rate and the carrier lifetime (Supplementary Note 1). For example, WS_2, with radiative and Auger lifetimes of ~50 µs and ~2 ms, respectively (Supplementary Table 3), exhibits ~2× larger radiative emission than SRH recombination, and negligible Auger loss.

Conclusions

We have examined the efficiency limits of multilayer TMD solar cells (MoS_2, $MoSe_2$, WS_2, and WSe_2) as a function of TMD film thickness and material quality, going beyond the Tiedje-Yablonovitch and Shockley-Queisser models by including experimental optical absorption spectra, as well as radiative, Auger and SRH recombination. We find that ultrathin TMD solar cells (as thin as 50 nm) can realistically achieve up to 25% power conversion efficiency even with today's material quality. This makes them an excellent choice for high-specific-power photovoltaics (i.e., with high power per weight), achieving up to 10× higher specific power than existing technologies. Such ultralight solar cells could transform energy harvesting across various industries including autonomous drones, electric vehicles, wearable electronics, and the Internet of Things. Future efforts must be dedicated to optimizing the electronic and optical TMD solar cell designs, to unlock their potential for high power conversion efficiency and specific power at large, industrial scale.

Methods

The detailed balance equation governing the current density–voltage characteristics of the solar cell and the method to extract the performance metrics, i.e., short-circuit current density, open-circuit voltage, fill factor, and power conversion efficiency, is explained in detail in Supplementary Note 1. The code developed to solve the detailed balance equation is provided in the Code availability section.

Data availability

The data that support the findings of this study are available from the corresponding author upon reasonable request.

Code availability

Code to replicate the main findings of this study can be found at https://doi.org/10.5281/zenodo.10291294.

Received: 26 May 2023; Accepted: 2 November 2023;
Published online: 20 December 2023

References

1. Reese, M. O. et al. Increasing markets and decreasing package weight for high-specific-power photovoltaics. *Nat. Energy* **3**, 1002–1012 (2018).

2. Jariwala, D., Davoyan, A. R., Wong, J. & Atwater, H. A. Van der Waals Materials for atomically-thin photovoltaics: promise and outlook. *ACS Photonics* **4**, 2962–2970 (2017).
3. Went, C. M. et al. A new metal transfer process for van der Waals contacts to vertical Schottky-junction transition metal dichalcogenide photovoltaics. *Sci. Adv.* **5**, eaax6061 (2019).
4. Nassiri Nazif, K. et al. High-specific-power flexible transition metal dichalcogenide solar cells. *Nat. Commun.* **12**, 7034 (2021).
5. Nassiri Nazif, K. et al. High-performance p–n junction transition metal dichalcogenide photovoltaic cells enabled by MoO_x doping and passivation. *Nano Lett.* **21**, 3443–3450 (2021).
6. Kim, K.-H. et al. High-efficiency WSe_2 photovoltaic devices with electron-selective contacts. *ACS Nano* **16**, 8827–8836 (2022).
7. Longo, R. C. et al. Intrinsic air stability mechanisms of two-dimensional transition metal dichalcogenide surfaces: basal versus edge oxidation. *2D Mater.* **4**, 25050 (2017).
8. Fojtů, M., Teo, W. Z. & Pumera, M. Environmental impact and potential health risks of 2D nanomaterials. *Environ. Sci. Nano* **4**, 1617–1633 (2017).
9. Das, S. et al. Transistors based on two-dimensional materials for future integrated circuits. *Nat. Electron.* **4**, 786–799 (2021).
10. Dorow, C. J. et al. Gate length scaling beyond Si: mono-layer 2D channel FETs robust to short channel effects. *In:* 2022 International Electron Devices Meeting (IEDM) 7.5.1–7.5.4 (2022).
11. Chung, Y.-Y. et al. First demonstration of GAA monolayer-MoS_2 nanosheet nFET with 410 μA/μm I_D at 1V V_D at 40nm gate length. *In:* 2022 International Electron Devices Meeting (IEDM) 34.5.1–34.5.4 (2022).
12. Wu, X. et al. Dual gate synthetic MoS_2 MOSFETs with 4.56μF/cm^2 channel capacitance, 320μS/μm G_m and 420 μA/μm I_d at 1 V V_d/100 nm L_g. *In:* 2021 IEEE International Electron Devices Meeting (IEDM) 7.4.1–7.4.4 (2021).
13. Tiedje, T., Yablonovitch, E., Cody, G. D. & Brooks, B. G. Limiting efficiency of silicon solar cells. *IEEE Trans. Electron Devices* **31**, 711–716 (1984).
14. Shockley, W. & Queisser, H. J. Detailed balance limit of efficiency of p-n junction solar cells. *J. Appl. Phys.* **32**, 510–519 (1961).
15. Yablonovitch, E. Statistical ray optics. *J. Opt. Soc. Am.* **72**, 899–907 (1982).
16. Yu, Z., Raman, A. & Fan, S. Fundamental limit of nanophotonic light trapping in solar cells. *Proc. Natl Acad. Sci.* **107**, 17491–17496 (2010).
17. Kravets, V. G. Ellipsometry and optical spectroscopy of low-dimensional family TMDs. *Semicond. Phys. Quantum Electron. Optoelectron.* **20**, 284–296 (2017).
18. Tauc, J., Grigorovici, R. & Vancu, A. Optical properties and electronic structure of amorphous germanium. *Phys. Status Solidi* **15**, 627–637 (1966).
19. Piprek, J. Efficiency droop in nitride-based light-emitting diodes. *Phys. Status Solidi* **207**, 2217–2225 (2010).
20. D'Rozario, J. R., Polly, S. J., Nelson, G. T., Wilt, D. & Hubbard, S. M. Modeling free-carrier absorption in ultrathin III-V solar cells with light management. *Opt. Express* **30**, 7096–7109 (2022).
21. McVay, E., Zubair, A., Lin, Y., Nourbakhsh, A. & Palacios, T. Impact of Al_2O_3 passivation on the photovoltaic performance of vertical WSe_2 Schottky junction solar cells. *ACS Appl. Mater. Interfaces* **12**, 57987–57995 (2020).
22. Weiss, T. P. et al. Bulk and surface recombination properties in thin film semiconductors with different surface treatments from time-resolved photoluminescence measurements. *Sci. Rep.* **9**, 5385 (2019).
23. Ramasubramaniam, A. Large excitonic effects in monolayers of molybdenum and tungsten dichalcogenides. *Phys. Rev. B* **86**, 115409 (2012).
24. Dias, A. C., Bragança, H., de Mendonça, J. P. A. & Da Silva, J. L. F. Excitonic effects on two-dimensional transition-metal dichalcogenide monolayers: impact on solar cell efficiency. *ACS Appl. Energy Mater.* **4**, 3265–3278 (2021).
25. Hu, Z., Lin, D., Lynch, J., Xu, K. & Jariwala, D. How good can 2D excitonic solar cells be? *Device* **1**, 100003 (2023).
26. Roy, S. & Bermel, P. Electronic and optical properties of ultra-thin 2D tungsten disulfide for photovoltaic applications. *Sol. Energy Mater. Sol. Cells* **174**, 370–379 (2018).
27. Roy, S., Hu, Z., Kais, S. & Bermel, P. Enhancement of photovoltaic current through dark states in donor-acceptor pairs of tungsten-based transition metal di-chalcogenides. *Adv. Funct. Mater.* **31**, 2100387 (2021).
28. Roy, S. & Bermel, P. Tungsten-disulfide-based ultrathin solar cells for space applications. *IEEE J. Photovolt.* **12**, 1184–1191 (2022).
29. Beal, A. R., Knights, J. C. & Liang, W. Y. Transmission spectra of some transition metal dichalcogenides. II. Group VIA: trigonal prismatic coordination. *J. Phys. C. Solid State Phys.* **5**, 3540 (1972).
30. Chernikov, A. et al. Exciton binding energy and nonhydrogenic rydberg series in monolayer WS2. *Phys. Rev. Lett.* **113**, 76802 (2014).
31. Vega-Mayoral, V. et al. Exciton and charge carrier dynamics in few-layer WS_2. *Nanoscale* **8**, 5428–5434 (2016).
32. Pedersen, T. G., Latini, S., Thygesen, K. S., Mera, H. & Nikolić, B. K. Exciton ionization in multilayer transition-metal dichalcogenides. *N. J. Phys.* **18**, 73043 (2016).
33. Palummo, M., Bernardi, M. & Grossman, J. C. Exciton radiative lifetimes in two-dimensional transition metal dichalcogenides. *Nano Lett.* **15**, 2794–2800 (2015).
34. Yuan, L. & Huang, L. Exciton dynamics and annihilation in WS_2 2D semiconductors. *Nanoscale* **7**, 7402–7408 (2015).
35. He, J. et al. Spatiotemporal dynamics of excitons in monolayer and bulk WS_2. *Nanoscale* **7**, 9526–9531 (2015).
36. Shi, H. et al. Exciton dynamics in suspended monolayer and few-layer MoS_2 2D crystals. *ACS Nano* **7**, 1072–1080 (2013).
37. Urbach, F. The long-wavelength edge of photographic sensitivity and of the electronic absorption of solids. *Phys. Rev.* **92**, 1324 (1953).
38. Sarangapani, P., Charles, J. & Kubis, T. Tuning band tails in mono- and multilayered transition-metal dichalcogenides: a detailed assessment and a quick-reference guide. *Phys. Rev. Appl.* **17**, 24005 (2022).
39. Li, Y. et al. Measurement of the optical dielectric function of monolayer transition-metal dichalcogenides: MoS_2, $MoSe_2$, WS_2, and WSe_2. *Phys. Rev. B* **90**, 205422 (2014).
40. Rühle, S. Tabulated values of the Shockley–Queisser limit for single junction solar cells. *Sol. Energy* **130**, 139–147 (2016).
41. Amani, M. et al. Recombination kinetics and effects of superacid treatment in sulfur- and selenium-based transition metal dichalcogenides. *Nano Lett.* **16**, 2786–2791 (2016).
42. Han, Y. et al. Photo-carrier lifetime in binary and ternary heterostructures of transition metal dichalcogenides. *Phys. Status Solidi* **260**, 2200501 (2023).
43. Pelant, I. & Valenta, J. Luminescence spectroscopy of semiconductors. Online edn. Oxford Academic, 24 May (2012).
44. Jakubowicz, A., Mahalu, D., Wolf, M., Wold, A. & Tenne, R. WSe_2: optical and electrical properties as related to surface passivation of recombination centers. *Phys. Rev. B* **40**, 2992–3000 (1989).
45. Memaran, S. et al. Pronounced photovoltaic response from multilayered transition-metal dichalcogenides PN-junctions. *Nano Lett.* **15**, 7532–7538 (2015).
46. Svatek, S. A. et al. High open-circuit voltage in transition metal dichalcogenide solar cells. *Nano Energy* **79**, 105427 (2021).
47. Green, M. A. Solar cell fill factors: general graph and empirical expressions. *Solid. State Electron.* **24**, 788–789 (1981).
48. Mialhe, P., Charles, J. P., Khoury, A. & Bordure, G. The diode quality factor of solar cells under illumination. *J. Phys. D. Appl. Phys.* **19**, 483 (1986).
49. Hall, R. N. Silicon photovoltaic cells. *Solid. State Electron.* **24**, 595–616 (1981).
50. Wickramaratne, D., Zahid, F. & Lake, R. K. Electronic and thermoelectric properties of few-layer transition metal dichalcogenides. *J. Chem. Phys.* **140**, 124710 (2014).

Acknowledgements

The authors acknowledge partial support from Stanford Precourt Institute for Energy and the member companies of the SystemX Alliance at Stanford.

Author contributions

K.N. and F.U.N. contributed equally. K.N. conceived the project. K.N. and F.U.N. developed the extended detailed balance model. F.U.N. implemented the model on TMDs, assisted by K.N. All authors, i.e., K.N., F.U.N., A.D., K.C.S, and E.P., contributed to the data interpretation, presentation, and writing of the manuscript. E.P. supervised the work.

Competing interests

The authors declare no competing interests.

Additional information

Supplementary information The online version contains supplementary material available at https://doi.org/10.1038/s42005-023-01447-y.

Correspondence and requests for materials should be addressed to Eric Pop.

Peer review information *Communications Physics* thanks the anonymous reviewers for their contribution to the peer review of this work.